

Optimal Nonlinear Eddy Viscosity in Galerkin Models of Turbulent Flows

Bartosz Protas^{1*}, Bernd R. Noack² and Jan Östh³

¹Department of Mathematics and Statistics
McMaster University, Hamilton, ON, Canada

²Institut PPRIME, CNRS - Université de Poitiers - ENSMA, UPR 3346
Département Fluides, Thermique, Combustion, CEAT
43 rue de l'Aérodrome, F-86036 Poitiers CEDEX, France

³Division of Fluid Dynamics, Department of Applied Mechanics
Chalmers University of Technology, SE-412 96 Göteborg, Sweden

December 3, 2024

Abstract

We propose a novel variational approach to identification of an optimal nonlinear eddy viscosity as a subscale turbulence representation for POD models. The ansatz for the eddy viscosity is given in terms of an arbitrary function of the resolved fluctuation energy. This function is found as a minimizer of a cost functional measuring the difference between the target data coming from a resolved direct or large-eddy simulation of the flow and its reconstruction based on the POD model. The optimization is performed with a data-assimilation approach generalizing the 4D-VAR method. POD models with optimal eddy viscosities are presented for a 2D incompressible mixing layer at $Re = 500$ (based on the initial vorticity thickness and the velocity of the high-speed stream) and a 3D Ahmed body wake at $Re = 300,000$ (based on the body height and the free-stream velocity). The variational optimization formulation elucidates a number of interesting physical insights concerning the eddy-viscosity ansatz used. The 20-dimensional model of the mixing-layer reveals a negative eddy-viscosity regime at low fluctuation levels which improves the transient times towards the attractor. The 100-dimensional wake model yields more accurate energy distributions as compared to the state-of-the-art nonlinear modal eddy-viscosity benchmark by Östh et al. (2014). Our methodology can be applied to construct quite arbitrary closure relations and,

*Email address for correspondence: bprotas@mcmaster.ca

more generally, constitutive relations optimizing statistical properties of a broad class of reduced-order models.

Keywords: Nonlinear Dynamics — Low-dimensional models; Mathematical Foundations — Variational methods; Turbulent Flows — Turbulence modelling; Wakes/jets — wakes.

1 Introduction

In this study we present an optimal nonlinear eddy-viscosity closure for flow models based on the proper orthogonal decomposition (POD). A reduced-order model (ROM) may serve as a testbed for physical understanding of actual flow phenomena, as a computationally inexpensive surrogate model for optimization and as a low-order plant for control design. The oldest quantitative ROMs are vortex models which are over 100 years old (see, e.g., Lamb, 1945). Most low-order vortex models of open flows are hybrid systems with a heuristic account of the creation, merging and annihilation of vorticity, and are thus not amenable to most approaches of system reduction, stability analysis, and control design. Many current ROMs of fluid flows are based on the traditional Galerkin method (see, e.g., Fletcher, 1984). In the kinematical step of this method, the flow is expanded in terms of N orthogonal basis functions \mathbf{u}_i , $i = 1, \dots, N$, as $\mathbf{u}(\mathbf{x}, t) = \sum_{i=1}^N a_i(t) \mathbf{u}_i(\mathbf{x})$. Thus, the mode coefficients $\mathbf{a}(t) = [a_1(t), \dots, a_N(t)]^T \in \mathbb{R}^N$ parameterize the fluid flow. The dynamical step consists in representing the dependent variables in the Navier-Stokes system in terms of such expansions and then projecting on the individual modes which leads to the Galerkin system in the general form

$$\frac{d\mathbf{a}}{dt} = \mathbf{f}(\mathbf{a}), \quad t > 0 \tag{1}$$

with propagator $\mathbf{f} : \mathbb{R}^N \rightarrow \mathbb{R}^N$. Many ROMs originate via post-processing of flow data obtained from simulations or experiments and rely on the proper orthogonal decomposition (see, e.g., Noack *et al.*, 2011; Holmes *et al.*, 2012). In the following, we focus on such POD models.

The error of the Galerkin model is expected to vanish for increasing dimension N . Since only a finite, and typically small, number of modes is retained, this procedure results in a loss of information. Hence, the reduced-order model (1) must be amended to restore some physical features. Generally, the large-scale coherent structures with the associated production of turbulent kinetic energy (TKE) are approximately resolved, while the small-scale fluctuations responsible for most of the dissipation are ignored. The resulting excess production of the fluctuation energy requires an additional stabilization in order to ensure the long-term boundedness of solutions of system (1). The need to introduce a suitable subscale turbulence representation gives rise to a “closure problem” analogous to the problem encountered when modeling turbulent flows based on the Reynolds-Averaged Navier-Stokes (RANS) equations and Large-Eddy Simulations

(LES), despite the fact that the latter two approaches rely on flow descriptions in terms of partial differential equations (PDEs), while system (1) is finite-dimensional. In particular, additional terms involving an “eddy viscosity” have been used in reduced-order models starting with the pioneering work of Aubry *et al.* (1988). These closure terms have been refined in numerous studies leading to, e.g., the modal eddy viscosities proposed by Rempfer & Fasel (1994*b*), calibration of an auxiliary linear term investigated by Galletti *et al.* (2004), a nonlinear term introduced by Cordier *et al.* (2013), combinations thereof studied by Östh *et al.* (2014), and projections of the filtered Navier-Stokes equation (Wang *et al.*, 2011), just to name only a few approaches. In addition, projections onto more dissipative subspaces were considered by Balajewicz *et al.* (2013). We refer the reader to Wang *et al.* (2012) for some new proposals and a critical assessment of several earlier approaches.

The discussed ROMs are all based on the Navier-Stokes equation. In principle, also the subscale closures can be derived from the first principles by means of structure and parameter identification. However, the availability of highly resolved numerical and experimental data sets makes data-driven modelling an appealing approach (see, e.g., Cacuci *et al.*, 2013; Kutz, 2013) and POD paves the way to this new modelling paradigm. Meanwhile, the parameters of Galerkin systems can be accurately identified with 4D VAR methods (Cordier *et al.*, 2013) and, in addition, closure relations may be inferred from measurements. A relatively recent development is the construction of subscale turbulence models based on optimization problems in which the closure model is adapted using available measurements. In the context of LES, this approach has been pioneered by Moser *et al.* leading to the concept of an “optimal LES” (Langford & Moser, 1999). Optimization-based formulations of the closure problem for Galerkin reduced-order models were recently pursued in D’Adamo *et al.* (2007); Artana *et al.* (2012); Cordier *et al.* (2013). In these studies the authors obtained time-dependent eddy viscosities $\nu_T = \nu_T(t)$ as minimizers of cost functionals representing the misfit between the measured and reconstructed data. However, the eddy viscosity obtained in this way is a function of time and the reduced-order model (1) is *no* longer autonomous which limits the practical applicability of such approaches. In this context, we also mention the recent study by Hemati *et al.* (2014) in which an analogous time-dependent closure was obtained for a vortex-based flow model.

In the present investigation we follow an optimization approach which is fundamentally different: the optimal eddy viscosity is sought as a function of the state \mathbf{a} , more precisely, its (turbulent) fluctuation energy $E(t) := \|\mathbf{a}(t)\|_2^2 = (1/2) \sum_{i=1}^N a_i(t)^2$, so that the resulting ROM (1) will then be *autonomous*. The proposed reconstruction approach is “non-parametric”, in the sense that no assumptions are made concerning the form of the dependence $\nu_T = \nu_T(E)$ other than smoothness and the limiting behavior for small and large values of E . Relying on the concepts of data assimilation, the proposed approach allows one to use measurement data in order to systematically refine nonlinear eddy viscosity models obtained theoretically. Therefore, it may be applicable to study the performance limitations of a given ansatz for the eddy viscosity. The method builds on the approach to the optimal reconstruction of constitutive relations in complex multi-

physics PDE problems developed by Bukshtynov *et al.* (2011) and Bukshtynov & Protas (2013). An application of this method to finite-dimensional Galerkin models was carefully validated using a 3-state ROM of laminar vortex shedding in the cylinder wake by Protas *et al.* (2014). In the present study, we employ this approach to identify optimal turbulence closures in two medium and high- Re flows, namely, a 2D incompressible mixing layer and a 3D wake flow behind a blunt-back Ahmed body. The dimensions of the corresponding Galerkin models are $N = 20$ for the mixing layer and $N = 100$ for the Ahmed body wake. In addition to offering predictability improvements over existing state-of-the-art approaches (Östh *et al.*, 2014), the optimal turbulence closures also reveal a number of unexpected yet physically plausible features, such as negative values of the eddy viscosity in some ranges of the turbulent kinetic energy E . We note that in fact the concept of a negative eddy viscosity has already been invoked in the studies of turbulent flows (see, e.g., Liberzon *et al.*, 2007).

The structure of the paper is as follows: In § 2 we briefly recapitulate POD Galerkin models and highlight some properties of the eddy viscosity in such models. Our computational approach is outlined in § 3. Optimal eddy viscosities and the properties of the resulting ROMs of the mixing layer and the Ahmed body flow are presented and analyzed in § 4. Summary and future directions are provided in § 5, whereas some technical material concerning the optimization approach is collected in Appendix A.

2 POD modeling

In this section, POD models for turbulent flows are briefly reviewed. First (§ 2.1), the assumed flow configurations are specified. The POD expansion and the corresponding Galerkin projection of the Navier-Stokes equation are described in §2.2 and § 2.3, respectively. In § 2.4, a nonlinear eddy viscosity ansatz is introduced against which the optimal relations of the next section will be benchmarked. Finally (§ 2.5), conditions for the appearance of negative values of eddy viscosity are identified thus setting the stage for the optimization formulation of § 3 and the initially somewhat surprising results reported in § 4.

2.1 Flow configurations

We assume an incompressible flow of a Newtonian fluid in a stationary domain Ω . The fluid is described by the density ρ and kinematic viscosity ν . The position and time are denoted \mathbf{x} and t , respectively. The flow field is described by the velocity \mathbf{u} and pressure p . The fluid motion is characterized by a velocity scale U and a length scale L defining the Reynolds number $Re = UL/\nu$. In the following, all quantities are assumed to be non-dimensionalized by U , L and ρ , and $\nu = 1/Re$ represents the reciprocal Reynolds number. The fluid motion is governed by the continuity equation and the momentum

balance

$$\nabla \cdot \mathbf{u} = 0, \quad (2a)$$

$$\partial_t \mathbf{u} + \mathbf{u} \cdot \nabla \mathbf{u} = -\nabla p + \nu \Delta \mathbf{u} \quad (2b)$$

subject to suitable initial and boundary conditions.

While the proposed methodology is fairly general, to fix attention, in this study we investigate two shear flows, a 2D spatially evolving mixing layer with a narrow frequency bandwidth and a 3D wake behind an Ahmed body with a broad frequency bandwidth including a slow drift of the base flow. In both flows, the origin of the Cartesian coordinate system is at the center of the inlet of the observation domain, i.e., is located at the maximum shear position in case of the mixing layer and at the center of the rear face of the Ahmed body. The x -axis points in the direction of the flow, the y -axis is aligned with the shear and the z -axis is orthogonal to the x - and y -coordinates.

2.2 Proper orthogonal decomposition

We perform a POD expansion (Lumley, 1970) of M velocity snapshots $\mathbf{u}^m := \mathbf{u}(\mathbf{x}, t^m)$ sampled at equispaced time instances $t^m = m\Delta t$, $m = 1, \dots, M$, with the time step Δt . The averaging operation of any velocity-dependent function $\mathbf{F}(\mathbf{u})$ over this ensemble is denoted by an overbar, i.e.,

$$\overline{\mathbf{F}(\mathbf{u})} := \frac{1}{M} \sum_{m=1}^M \mathbf{F}(\mathbf{u}^m). \quad (3)$$

(“:=” means that the left-hand side of the equation is defined by the right-hand side). The inner product for two velocity fields $\mathbf{v}, \mathbf{w} \in L_2(\Omega)$ is defined as

$$\langle \mathbf{v}, \mathbf{w} \rangle_{L_2(\Omega)} := \int_{\Omega} \mathbf{v} \cdot \mathbf{w} \, d\mathbf{x}. \quad (4)$$

This inner product defines the energy norm $\|\mathbf{v}\|_{L_2(\Omega)} = \sqrt{\langle \mathbf{v}, \mathbf{v} \rangle_{L_2(\Omega)}}$.

The averaging operation and the inner product uniquely define the corresponding snapshot POD (Sirovich, 1987; Holmes *et al.*, 2012). First, following the Reynolds decomposition, the velocity field is decomposed into a mean field, $\mathbf{u}_0 := \overline{\mathbf{u}}$, and a fluctuating contribution $\mathbf{u}' := \mathbf{u} - \overline{\mathbf{u}}$. Then, the fluctuating part is approximated by a Galerkin expansion with space-dependent modes $\mathbf{u}_i(\mathbf{x})$, $i = 1, 2, \dots, N$, used as the basis function and the corresponding mode coefficients $a_i(t)$

$$\mathbf{u}(\mathbf{x}, t) = \mathbf{u}_0(\mathbf{x}) + \sum_{i=1}^N a_i(t) \mathbf{u}_i(\mathbf{x}) + \mathbf{u}_{res}(\mathbf{x}, t), \quad (5)$$

where \mathbf{u}_{res} represents the residual. POD yields a Galerkin expansion with the minimal average squared residual $\|\mathbf{u}_{res}\|_{L_2(\Omega)}^2$ as compared to any other Galerkin expansion with

N modes (Lumley, 1970). We note that the snapshot POD method limits the number of POD modes to $N \leq M - 1$.

To facilitate subsequent developments, we rewrite the POD expansion more compactly following the convention of Rempfer & Fasel (1994*a,b*):

$$\mathbf{u}(\mathbf{x}, t) = \sum_{i=0}^N a_i(t) \mathbf{u}_i(\mathbf{x}), \quad (6)$$

where $a_0(t) \equiv 1$ (because of this property we will refer to the phase space as N -dimensional, even though the state vector $\mathbf{a}(t)$ has formally the dimension $N + 1$). For later reference, we recapitulate the first and second moments of the POD mode coefficients:

$$\overline{a_i} = 0, \quad \overline{a_i a_j} = \lambda_i \delta_{ij}, \quad i, j = 1, \dots, N, \quad (7)$$

where λ_i are the POD eigenvalues. The energy content in each mode is given by $E_i(t) := a_i^2(t)/2$ and the turbulent kinetic energy resolved by the Galerkin expansion $E(t)$ is

$$E(t) = \sum_{i=1}^N E_i(t). \quad (8)$$

At any fixed time t , the limit $\lim_{N \rightarrow \infty} E(t)$ for POD yields the total turbulent kinetic energy $K(t)$ of the original velocity field. We note that, by (7), the average modal energy and POD eigenvalues are synonymous: $\overline{E_i} = \lambda_i/2$.

2.3 Galerkin projection

The Galerkin expansion (6) satisfies the incompressibility condition and the boundary conditions by construction. The evolution equation for the mode coefficients a_i is derived by a *Galerkin projection* of the Navier-Stokes equation (2) written in the operator form as $\mathbf{R}(\mathbf{u}) = \mathbf{0}$ onto individual POD modes, i.e., via $\langle \mathbf{u}_i, \mathbf{R}(\mathbf{u}) \rangle_{L^2(\Omega)} = 0$, $i = 1, \dots, N$. Details are provided in the monographs by Noack *et al.* (2011) and Holmes *et al.* (2012). For internal flows, the Galerkin representation of the pressure term vanishes. For open flows with large domains and three-dimensional fluctuations, the pressure term can generally be neglected as discussed by Deane *et al.* (1991), Ma & Karniadakis (2002) and Noack *et al.* (2005). Here, the Galerkin projection of the pressure term was found to be negligible and it is therefore omitted from the model. Thus, the Galerkin system describing the temporal evolution of the modal coefficients, $a_i(t)$, reads

$$\frac{da_i}{dt} = f_i(\mathbf{a}) = \nu \sum_{j=0}^N l_{ij}^\nu a_j + \sum_{j,k=0}^N q_{ijk}^c a_j a_k, \quad i = 1, \dots, N. \quad (9)$$

The coefficients l_{ij}^ν and q_{ijk}^c , $i, j, k = 0, \dots, N$, are the Galerkin coefficients describing, respectively, the viscous and convective effects in the Navier-Stokes system (2). For

internal flows with the Dirichlet or periodic boundary conditions, the quadratic term can be shown to be exactly energy-preserving

$$q_{ijk}^c + q_{ikj}^c + q_{kij}^c + q_{kji}^c + q_{jik}^c + q_{ikj}^c = 0, \quad i, j, k = 1, \dots, N. \quad (10)$$

For open flows, this is still found to be a good approximation.

2.4 Post-transient fluctuation levels

For turbulent flows, POD models face one well-known challenge addressed already in the pioneering work of Aubry *et al.* (1988): the finite POD expansion often contains a fraction of the total fluctuation energy. While a significant portion of the TKE production may be resolved by the large-scale structures contained in the POD expansion, most of the dissipation in the small-scale eddies is ignored in the Galerkin system. The resulting over-production of TKE in the POD model leads to over-prediction of the fluctuation level, including possible divergence to infinity in finite time. A common cure is the inclusion of an “eddy viscosity” term absorbing the excess energy,

$$\frac{da_i}{dt} = f_i(\mathbf{a}) + \nu_T \sum_{j=0}^N l_{ij}^{\nu} a_j, \quad i = 1, \dots, N. \quad (11)$$

Generally, off-diagonal elements l_{ij}^{ν} , $i \neq j$, are small and therefore negligible.

In early studies eddy viscosity ν_T was assumed to be a constant parameter. Yet, the non-physical implication is that the POD-resolved part of the turbulent flow effectively behaves like a laminar flow with reciprocal Reynolds number $\nu_{\text{eff}} = \nu + \nu_T$. Another non-physical implication is that a *linear* Galerkin term is to represent the *nonlinear* energy cascade. Numerous refinements of this eddy viscosity term have been suggested as discussed by Östh *et al.* (2014). In this study, our point of departure is a nonlinear modal eddy viscosity

$$\nu_T^{\circ} = \nu_T^a \sqrt{\frac{E(t)}{\bar{E}}} \kappa_i \quad (12)$$

with the mode-dependent factor κ_i , $i = 1, \dots, N$. This factor is equal to the unity, $\kappa_i \equiv 1$, for the global eddy-viscosity ansatz and is derived from the modal power balance of the flow (Noack *et al.*, 2005) for the modal eddy viscosity. The eddy viscosity ν_T° becomes larger (smaller) than the reference value ν_T^a characterizing the flow attractor when the instantaneous resolved fluctuation energy $E(t)$ is larger (smaller) than the reference. The square-root dependency of ν_T° on $E(t)$ in (12) is motivated by a scaling argument (Noack *et al.*, 2011) and we add that this nonlinear eddy viscosity term guarantees the boundedness of any Galerkin solution (Cordier *et al.*, 2013).

2.5 Transient dynamics

The nonlinear eddy viscosity term effectively has the ability to prevent non-physically large fluctuation levels. Another frequently observed shortcoming of POD systems are

significantly over-predicted transient times, even for laminar flows. To shed light on this issue and show how it can be remedied through a suitable choice of a nonlinear eddy viscosity, in the following we consider one of the simplest POD Galerkin models exhibiting non-physical transient times *and* non-physical fluctuation levels. The starting point is the 2D laminar cylinder wake at $Re = 100$ in an unbounded domain truncated for computational purposes to a finite box (Noack *et al.*, 2003). The first two POD modes resolve already 95% of the fluctuation energy and we chose $N = 2$ as the model order. The POD system is effectively phase-invariant and is well approximated by a linear oscillator:

$$\dot{a}_1 = f_1(a_1, a_2) = \sigma^\circ a_1 - \omega^\circ a_2, \quad (13a)$$

$$\dot{a}_2 = f_2(a_1, a_2) = \sigma^\circ a_2 + \omega^\circ a_1, \quad (13b)$$

$$\sigma^\circ = 0.0073, \quad (13c)$$

$$\omega^\circ = 1.0763. \quad (13d)$$

The quadratic term vanishes by (10) and the observed phase invariance. Evidently, (13) describes an oscillatory behaviour with a slow exponential growth, i.e., growth without bound.

The mode coefficients a_i^\bullet , $i = 1, 2$, obtained from a direct numerical simulation (DNS) starting from the steady solution quickly converge to a limit cycle. This transient is far better approximated by the following mean-field model exhibiting a stable limit cycle at $r_\infty \approx 2.3$ (Protas *et al.*, 2014):

$$\dot{a}_1 = \sigma^\bullet a_1 - \omega^\bullet a_2, \quad (14a)$$

$$\dot{a}_2 = \sigma^\bullet a_2 + \omega^\bullet a_1, \quad (14b)$$

$$\sigma^\bullet = \sigma_1 [1 - r^2/r_\infty^2], \quad (14c)$$

$$\omega^\bullet = \omega_1 + 0.150 r^2/r_\infty^2. \quad (14d)$$

with $\sigma_1 = 0.151$ and $\omega_1 = 0.886$ representing the initial growth rate and frequency of the transient solution, and $r := \sqrt{a_1^2 + a_2^2}$.

The growth rate (13c) of the POD model is thus initially underpredicted by more than a factor of 20 while it is increasingly overpredicted near and beyond the limit cycle. We aim to correct this growth rate using the eddy viscosity ansatz of the form (11) which results in:

$$\dot{a}_1 = f_1(a_1, a_2) + \nu_T l_{11}^\nu a_1, \quad (15a)$$

$$\dot{a}_2 = f_2(a_1, a_2) + \nu_T l_{22}^\nu a_2. \quad (15b)$$

Here, $l_{11}^\nu = l_{22}^\nu < 0$ by the assumed phase invariance and the dissipativity property of the viscous term. Matching the growth rate of (15) with the DNS-inferred mean-field model (14) yields

$$\nu_T |l_{11}^\nu| = \sigma^\bullet - \sigma^\circ = \sigma_1 [1 - r^2/r_\infty^2] - \sigma^\circ$$

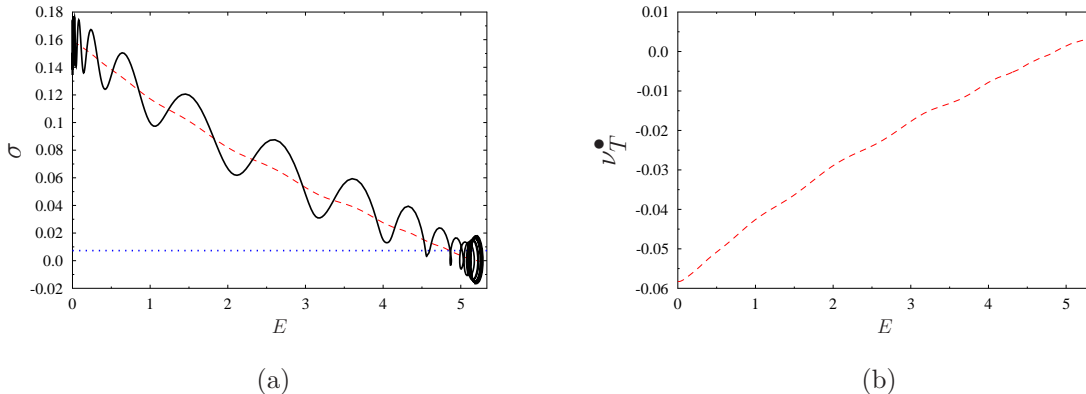


Figure 1: Results obtained for the two-dimensional cylinder wake flow at $Re = 100$: (a) the growth rates σ in reduced-order models (13)–(14) and (b) the corresponding optimal eddy viscosity ν_T^\bullet in system (15) as functions of the fluctuation energy E ; optimal reconstructions σ^\bullet and ν_T^\bullet (red dashed lines), prediction from Galerkin model (13) (blue dotted line) and the quantity $r^{-1}(dr/dt)|_{r(t)}$ computed based on the solution of the Navier-Stokes problem (black solid line).

Evidently, the eddy viscosity is an affine function of the fluctuation energy $E(t) = r(t)^2/2$, i.e.,

$$\nu_T(E) = a + bE \quad (16)$$

with a negative intercept $a = (\sigma^\circ - \sigma_1)/l_{11}^\nu$ and a positive slope $b = \sigma_1/(E_\infty l_{11}^\nu)$, in which $E_\infty = \overline{(a_1^2 + a_2^2)}/2 = r_\infty^2/2$, so that $\nu_T = -\sigma_1/l_{11}^\nu > 0$ at $E = E^a$, where E^a is the fluctuating energy level corresponding to the attractor. Figure 1 illustrates these observations by showing the growth rates of the POD model, generalized mean-field model of Protas *et al.* (2014) and the corresponding eddy viscosities. We note that the form of (16) as an affine function of E is different from (12) which involves a square-root expression. There is, however, no contraction, since (12) is obtained for the flow energy cascade with triadic mode interactions, while the mean-field model (14) describes the change of the growth rate due to base-flow variations with the associated Reynolds stresses proportional to E .

Summarizing, a negative (positive) eddy viscosity at low (large) fluctuation values can cure non-physically long transient times to the attractor. In the following we thus allow the eddy viscosity to be an essentially arbitrary function of E

$$\nu_T^\bullet := \nu_T^\bullet(E). \quad (17)$$

In the light of the cylinder wake example, one may therefore expect small or negative values of the eddy viscosity to arise for $E < \overline{E}$ and positive values for $E > E^a$.

The marginal growth rates of POD models may be also related to unresolved base flow variations (Aubry *et al.*, 1988; Podvin, 2009; Noack *et al.*, 2003) and mode deformation

during transients (Noack *et al.*, 2003; Sapsis & Majda, 2013). While it is possible to address these issues in our framework, it would significantly complicate the exposition, hence they will not be considered in the present study.

3 Optimal eddy viscosity

In this section we describe a variational approach for determination of an *optimal* dependence of the nonlinear eddy viscosity ν_T in the Galerkin system (11) on the turbulent kinetic energy E . Here, “optimality” means that the eddy viscosity minimizes a performance criterion quantifying how well the evolution described by reduced-order model (11) matches the actual evolution governed by Navier-Stokes system (2). We assume that over some time window $t \in [0, T]$ the flow is characterized by the resolved turbulent kinetic energy $\tilde{E}(t)$ representing the energy content of its first N POD modes, i.e.,

$$\tilde{E}(t) := \frac{1}{2} \sum_{i=1}^N \langle \mathbf{u}'(\cdot, t), \mathbf{u}_i \rangle_{L_2(\Omega)}^2. \quad (18)$$

This fluctuation energy is determined from the solution (here, DNS or LES) of the Navier-Stokes problem. Then, we can define the following cost functional

$$\mathcal{J}(\nu_T) = \frac{1}{2T} \int_0^T \left[E(t; \nu_T) - \tilde{E}(t) \right]^2 dt, \quad (19)$$

where $E(t; \nu_T)$ is the turbulent kinetic energy characterizing system (11) which depends on eddy viscosity ν_T . Since the length T of the time window on which measurements $\tilde{E}(t)$ are available can be quite long compared to the times over which the reduced-order model (11) is capable of reproducing accurately the actual trajectory, in evaluating $E(t; \nu_T)$ we will periodically restart system (11) using projections of the actual flow evolution on the POD modes as the initial data \mathbf{a}^0 . More precisely, we will subdivide the interval $[0, T]$ into M subintervals of length $\Delta T = T/M$, so that $[0, T] = [0, \Delta T] \cup [\Delta T, 2\Delta T] \cup \dots \cup [(M-1)\Delta T, M\Delta T]$, see figure 2. On each of the subintervals $[(m-1)\Delta T, m\Delta T]$, $m = 1, \dots, M$, the Galerkin system will therefore take the form

$$\frac{da_i}{dt} = \sum_{j,k=0}^N q_{ijk}^c a_j a_k + [\nu + \nu_T(E(t))] \sum_{j=0}^N l_{ij}^v a_j, \quad t \in ((m-1)\Delta T, m\Delta T] \quad (20a)$$

$$a_i((m-1)\Delta T) = a_i^{0,m}, \quad i = 1, \dots, N, \quad (20b)$$

where $a_i^{0,m} = \langle \mathbf{u}'(\cdot, (m-1)\Delta T), \mathbf{u}_i \rangle_{L_2(\Omega)}$ and $m = 1, \dots, M$.

The nonlinear eddy viscosity ν_T° introduced in § 2.4, cf. (12), will serve as a reference and point of departure for the present optimization approach. As regards the functional form of the optimal eddy viscosity ν_T^\bullet , we will make the following rather unrestrictive assumptions (hereafter we will use the symbol e as the variable corresponding to the turbulent kinetic energy E).

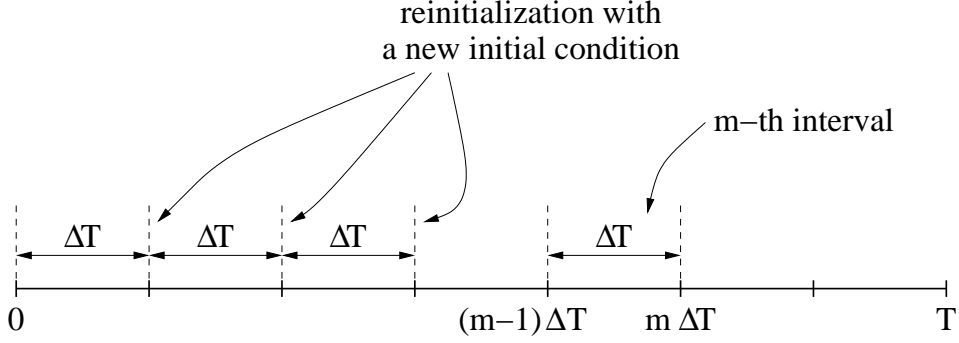


Figure 2: Schematic showing the partition of the time window $[0, T]$ into subintervals $[(m-1)\Delta T, m\Delta T]$, $m = 1, \dots, M$.

Assumption 1 1. $\nu_T^\bullet(e)$ is defined for $e \in \mathcal{I} := [0, E_{max}]$, where E_{max} is chosen such that $E_{max} > \max_{t \in [0, T]} E(t)$,

2. $\nu_T^\bullet(e)$ is a continuous function of e with square-integrable derivatives on \mathcal{I} ; this implies that $\nu_T^\bullet \in H^1(\mathcal{I})$, where $H^1(\mathcal{I})$ is the Sobolev function space equipped with the inner product (Adams & Fournier, 2005)

$$\forall_{z_1, z_2 \in H^1(\mathcal{I})} \quad \langle z_1, z_2 \rangle_{H^1(\mathcal{I})} = \int_0^{E_{max}} z_1 z_2 + \ell^2 \frac{\partial z_1}{\partial e} \frac{\partial z_2}{\partial e} de, \quad (21)$$

where $\ell > 0$,

3.

$$\nu_T^\bullet(0) = \nu_T^\circ(0) = 0, \quad (22)$$

4.

$$\left. \frac{d\nu_T^\bullet}{de} \right|_{e=E_{max}} = \left. \frac{d\nu_T^\circ}{de} \right|_{e=E_{max}} =: G, \quad (23)$$

implying that for large values of the turbulent kinetic energy e the behavior of the optimal eddy viscosity ν_T^\bullet will be consistent with the behavior of theoretical model ν_T° .

It should be emphasized that the eddy viscosity ν_T is allowed to become negative for some values of the turbulent kinetic energy e .

The optimization problem for finding ν_T^\bullet can be therefore stated as follows

$$\nu_T^\bullet = \underset{\nu_T \in H^1(\mathcal{I}), \nu_T(0)=0, \left. \frac{d\nu_T}{de} \right|_{e=E_{max}} = G}{\operatorname{argmin}} \quad \mathcal{J}(\nu_T) \quad (24)$$

with cost functional $\mathcal{J}(\nu_T)$ given in (19) together with (20). While problem (24) is of the “parameter identification” type, it is in fact quite different from the related problems already studied in the literature on reduced-order modelling (D’Adamo *et al.*, 2007;

Artana *et al.*, 2012; Cordier *et al.*, 2013), in which the optimal eddy viscosity ν_T was sought as a function of time (i.e., an independent variable in the problem). The resulting reduced-order model is *non-autonomous* and therefore restricted to the time-window and the initial condition used in the determination of the optimal eddy viscosity. Consequently, such time-dependent optimal eddy viscosity cannot be considered a proper “closure model”. On the other hand, formulation (24) leads to an optimal eddy viscosity as a constitutive relation of the form $\nu_T^\bullet = \nu_T^\bullet((1/2)\|\mathbf{a}\|_2^2)$ and the corresponding reduced-order model is *autonomous*.

In order to ensure that optimal eddy viscosity ν_T^\bullet satisfies Assumption 1, we will adopt the “optimize-then-discretize” paradigm (Gunzburger, 2003) in solving problem (24). While solution of this problem relies on a standard gradient-based approach, it requires a specialized technique for the evaluation of gradients. Its mathematical and computational foundations were established by Bukshtynov *et al.* (2011) and Bukshtynov & Protas (2013), and here we use an adaptation of this approach to the identification of reduced-order models recently developed by Protas *et al.* (2014). Below we present the main elements of the algorithm deferring technical details to Appendix A.

The (local) minimizer ν_T^\bullet of (19) is characterized by the first-order optimality condition (Luenberger, 1969) requiring the vanishing of the Gâteaux differential $\mathcal{J}'(\nu_T; \nu_T') := \lim_{\epsilon \rightarrow 0} \epsilon^{-1} [\mathcal{J}(\nu_T + \epsilon \nu_T') - \mathcal{J}(\nu_T)]$, i.e.,

$$\forall_{\nu_T' \in H^1(\mathcal{I}), \nu_T'(0)=0, \left. \frac{d\nu_T'}{de} \right|_{e=E_{\max}} = 0} \quad \mathcal{J}'(\nu_T^\bullet; \nu_T') = 0, \quad (25)$$

where ν_T' is an arbitrary perturbation direction. This minimizer can be computed as $\nu_T^\bullet = \lim_{n \rightarrow \infty} \nu_T^{(n)}$ using the following iterative procedure

$$\begin{cases} \nu_T^{(n+1)} = \nu_T^{(n)} - \tau^{(n)} \nabla \mathcal{J}(\nu_T^{(n)}), & n = 1, \dots, \\ \nu_T^{(1)} = \nu_T^\circ, \end{cases} \quad (26)$$

where the reference eddy viscosity ν_T° from § 2.4 is taken as the initial guess, n denotes the iteration count and $\nabla \mathcal{J} : \mathcal{I} \rightarrow \mathbb{R}$ is the gradient of cost functional \mathcal{J} . The length $\tau^{(n)}$ of the step is determined by solving line minimization problem

$$\tau^{(n)} = \underset{\tau > 0}{\operatorname{argmin}} \mathcal{J} \left(\nu_T^{(n)} - \tau \nabla \mathcal{J}_1(\nu_T^{(n)}) \right) \quad (27)$$

which can be done efficiently using standard techniques such as Brent’s method (Press *et al.*, 1986). For the sake of clarity, formulation (26) represents the steepest-descent method, however, in practice one typically uses more advanced minimization techniques, such as the conjugate gradient method, or one of the quasi-Newton techniques (Nocedal & Wright, 2002). Evidently, the key element of minimization algorithm (26) is the computation of the cost functional gradient $\nabla \mathcal{J}$. It ought to be emphasized that, while the governing system (20) is finite-dimensional, the gradient $\nabla \mathcal{J}$ is a function of the turbulent kinetic

energy E and as such represents a continuous (infinite-dimensional) sensitivity of cost functional $\mathcal{J}(\nu_T)$ to the perturbations $\nu'_T = \nu'_T(E)$. As shown in Appendix A, the L_2 gradient of cost functional (19) can for $e \in [0, E_{\max}]$ be evaluated as

$$\nabla^{L_2} \mathcal{J}(e) = \sum_{E(\mathbf{a}(t))=e} \frac{\sum_{i,j=0}^N l_{ij}^\nu a_j(t) a_i^*(t)}{\sum_{i=1}^N a_i(t) \left[f_i(\mathbf{a}(t)) + \nu_T((1/2)\|\mathbf{a}(t)\|_2^2) \sum_{j=0}^N l_{ij}^\nu a_j(t) \right]} \quad (28)$$

in which $f_i(\mathbf{a}(t))$ is defined in (9), whereas $\mathbf{a}^*(t) = [0, a_1^*(t), \dots, a_N^*(t)]^T \in \mathbb{R}^{N+1}$ is the solution of adjoint system

$$-\frac{da_i^*}{dt} = \sum_{j=0}^N A_{ji} a_j^* + \frac{a_i}{T} \left[E(t) - \tilde{E}(t) \right], \quad t \in ((m-1)\Delta T, m\Delta T] \quad (29a)$$

$$a_i^*(m\Delta T) = 0, \quad i = 1, \dots, N, \quad m = 1, \dots, M, \quad (29b)$$

where \mathbf{A} is the linearized operator defined in Appendix A. So that it has the same dimension $(N+1)$ as the state vector $\mathbf{a}(t)$, cf. §2.2, the adjoint state $\mathbf{a}^*(t)$ is defined to have an extra (zero) element in the first position. In order to ensure that the optimal eddy viscosity ν_T^\bullet possesses the smoothness and boundary behavior required by Assumption 1, in iterations (26) we need to use the H^1 Sobolev gradient $\nabla \mathcal{J} = \nabla^{H^1} \mathcal{J}$ defined with respect to inner product (21), rather than the L_2 gradient given in (28). The two gradients are related through the following elliptic boundary-value problem (Protas *et al.*, 2004)

$$\left(1 - \ell^2 \frac{d^2}{de^2} \right) \nabla^{H^1} \mathcal{J} = \nabla^{L_2} \mathcal{J} \quad \text{in } (0, E_{\max}), \quad (30a)$$

$$\nabla^{H^1} \mathcal{J} = 0 \quad \text{at } e = 0, \quad (30b)$$

$$\frac{d}{de} \nabla^{H^1} \mathcal{J} = 0 \quad \text{at } e = E_{\max}, \quad (30c)$$

where $\ell \in \mathbb{R}$ is a parameter with the meaning of a “length scale”. Protas *et al.* (2004) showed that extraction of cost functional gradients in the space H^1 with the inner product defined as in (21) can be regarded as low-pass filtering the L_2 gradients with the cut-off wavenumber given by ℓ^{-1} . As regards the behavior of the gradients $\nabla^{H^1} \mathcal{J}$ at the endpoints of the interval \mathcal{I} , boundary conditions (30b)–(30c) ensure that all iterates $\nu_T^{(n)}$ have the same behavior as the initial guess ν_T° , cf. Assumption 1(c,d). At every iteration (26) of the computational algorithm one first evaluates the L_2 gradient (28), which requires integration along the system trajectory in the phase space \mathbb{R}^N (Protas *et al.*, 2014), and then solves problem (30) as a “post-processing” step to obtain the Sobolev gradient $\nabla^{H^1} \mathcal{J}$. Application of this approach to identification of the optimal eddy viscosity in reduced-order models of two complex flow problems is discussed in the next section.

4 Results

In this section we present the results obtained applying the procedure from § 3 to determine the optimal eddy viscosity ν_T^\bullet for two realistic flow problems with distinct properties from the point of view of reduced-order modeling. The first one, discussed in § 4.1, concerns a 2D mixing layer at a medium Reynolds number. It features a small number of dominating frequencies and most of the flow energy is resolved by a 20-dimensional Galerkin model. The second problem, discussed in §4.2, concerns a high Reynolds number wake flow past an Ahmed body. This flow problem is characterized by a broadband frequency spectrum such that a 100-dimensional Galerkin model resolves less than half of the total energy only.

4.1 Mixing layer model

The 2D mixing layer has a Reynolds number of 500 based on the initial vorticity thickness $L = \delta_v$ and the maximum velocity of the upper stream $U = U_1$. The velocity ratio between the upper and lower stream is $U_1/U_2 = 3$. The observation region for the POD analysis is a subset of the computational domain and given by

$$\Omega := \{(x, y) : 0 \leq x \leq 140, \quad -28 \leq y \leq 28\}. \quad (31)$$

The post-transient flow is computed over 2000 convective time units and sampled with the uniform time step $\Delta t = 1$. Details of the direct Navier-Stokes simulations (DNS) are described by Kasten *et al.* (2014); Kaiser *et al.* (2014), and figure 3 shows snapshot of the vorticity field in the flow. The numerical data is used to construct Galerkin system (11) with dimension $N = 20$ using the procedure discussed in § 2 and setting $\kappa_i = 1$, $i = 1, \dots, N$, in (12). The dimension $N = 20$ ensures that the Galerkin system captures 80% of the flow energy. Optimization problem (24) is solved for a broad range of time intervals $4 \leq \Delta T \leq 2000$ ($500 \geq M \geq 1$) at which the governing system (20) is restarted with new initial conditions. In order to illustrate the behavior of our approach, below we will present the results for two representative cases with $\Delta T = 10$ and $\Delta T = 200$ which will be referred to as optimization over, respectively, short and long windows.

We begin by presenting in figure 4 the decrease of cost functional (19) with iterations (26). We see that in the case of the short window ($\Delta T = 10$) not only are the values of functional (19) smaller, but also the relative decrease achieved during iterations is less significant (about 8% in figure 4a). This implies that over such short time windows the physical ansatz (12) for eddy viscosity performs satisfactorily and the improvement obtained with optimization is marginal only. On the other hand, in the case with longer time windows ($\Delta T = 200$, see figure 4b), the values of the cost functional are much larger as is its relative reduction (about 74%) achieved with optimization. The corresponding optimal eddy viscosities ν_T^\bullet are presented in figure 5 together with the theoretical relation (12). We see that the main modification with respect to ν_T° takes place for $E \in [0, 100]$ which is the range of values spanned by the DNS solution, see figure 6a, whereas for values of E outside that range the modifications of the eddy viscosity are essentially the

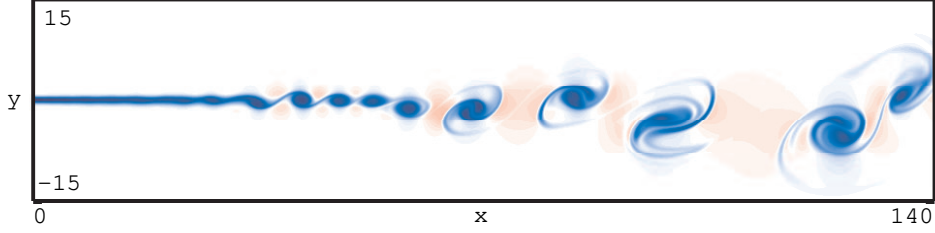


Figure 3: An instantaneous vorticity field (with red and blue representing, respectively, positive and negative values) in the 2D mixing layer flow studied in § 4.1.

effect of Assumption 1. Two distinct behaviours are observed, with the optimal eddy viscosity ν_T^\star becoming negative for $E \in [0, 40]$ in the case with optimization over long windows ($\Delta T = 200$). We remark that this feature of the eddy viscosity was already discussed in § 2.5 where it was found to arise in a two-dimensional Galerkin model of laminar vortex shedding in the cylinder wake.

The histories of the resolved total kinetic energy $E(t)$, which is the quantity used as the performance criterion in our optimization problem, cf. (19), are presented in figure 6a, whereas in figure 6b we show the corresponding average modal energies \bar{E}_i , $i = 1, \dots, 20$. The mean values of the total kinetic energy \bar{E} and their standard deviations are summarized in Table 1. From the data in figure 6 and Table 1 we see that the optimal eddy viscosity ν_T^\star obtained with optimization over long windows ($\Delta T = 200$) allows Galerkin system (11) to track the total kinetic energy $\tilde{E}(t)$ of the original DNS simulation much better than when the physical ansatz ν_T^o is used. On the other hand, when the optimal eddy viscosity is obtained with optimization over short windows ($\Delta T = 10$), only a modest improvement is observed. These observations are also corroborated by the results presented in figure 7, where we show the time-histories of selected Galerkin coefficients $a_i(t)$, $i = 1, 5, 10, 20$, and in figure 8 where we present the “unbiased” correlation function (Orfanidis, 1996)

$$C(\tau) := \frac{1}{T - \tau} \int_{\tau}^T \langle \mathbf{u}'(\cdot, t - \tau) \cdot \mathbf{u}'(\cdot, t) \rangle_{L_2(\Omega)} dt, \quad \tau \in [0, T) \quad (32)$$

after normalization with respect to $C(0)$. We note that using ansatz (5) and the orthogonality property of the POD modes, it can be conveniently evaluated in terms of the autocorrelations of the individual Galerkin coefficients, i.e.,

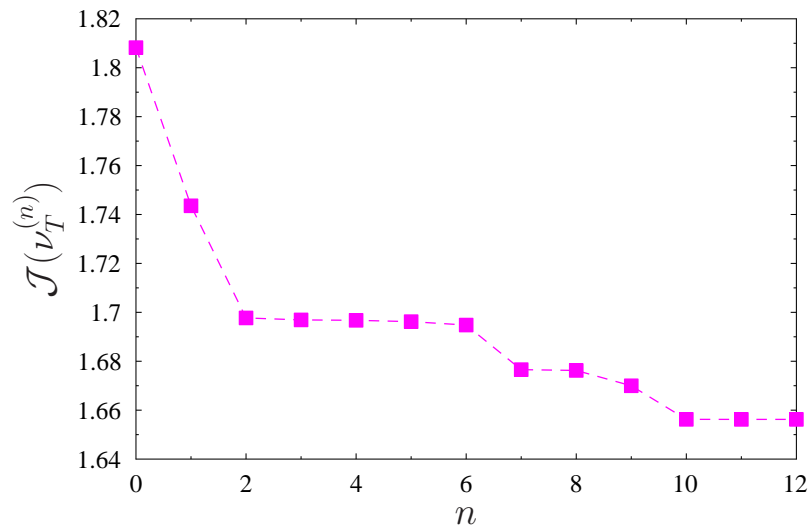
$$C(\tau) = \frac{1}{T - \tau} \sum_{i=1}^N \int_{\tau}^T a_i(t - \tau) a_i(t) dt. \quad (33)$$

Finally, in figure 9 we compare our results concerning the history of the total kinetic energy $E(t)$ with the results obtained by Cordier *et al.* (2013) who used an optimization

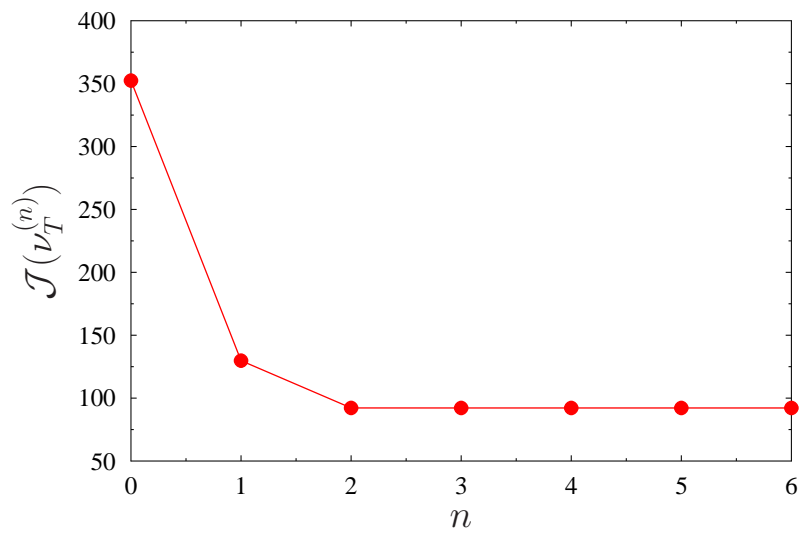
Table 1: [Mixing layer] Mean resolved turbulent kinetic energy \overline{E} and its standard deviation $std(E)$ in the different cases considered in § 4.1.

	Original DNS ($N = 20$)	System (11) with ν_T°	System (11) with ν_T^\bullet short windows ($\Delta T = 10$)	System (11) with ν_T^\bullet long windows ($\Delta T = 200$)
\overline{E}	61.73	58.43	80.84	51.27
$std(E)$	20.12	24.79	23.77	13.41

approach to determine eddy viscosities as functions of time $\nu_T = \nu_T(t)$ with different cost functionals. We see that the optimization formulation proposed here, in which the optimal eddy viscosity is sought as a function of the instantaneous turbulent kinetic energy $\nu_T^\bullet = \nu_T^\bullet(E)$, clearly leads to better results.



(a)



(b)

Figure 4: [Mixing layer] Decrease of the cost functional (19) with iterations n for optimization over (a) over short windows ($\Delta T = 10$) and (b) over long windows ($\Delta T = 200$).

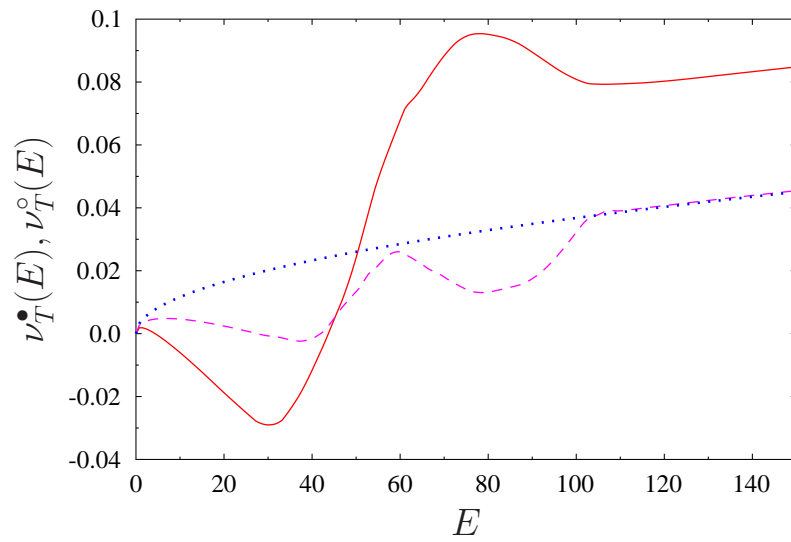
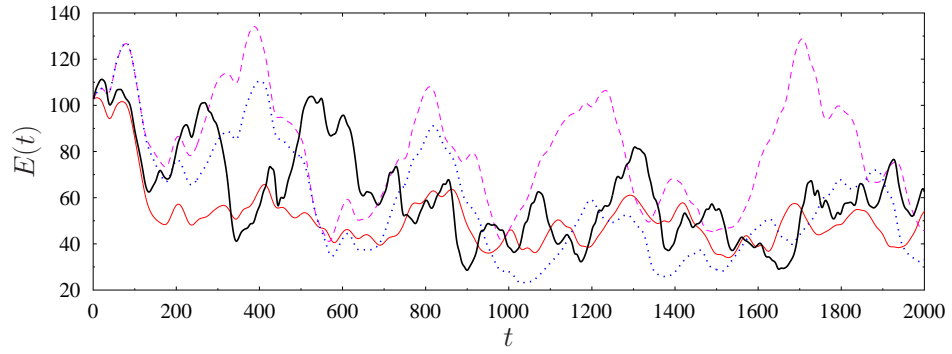
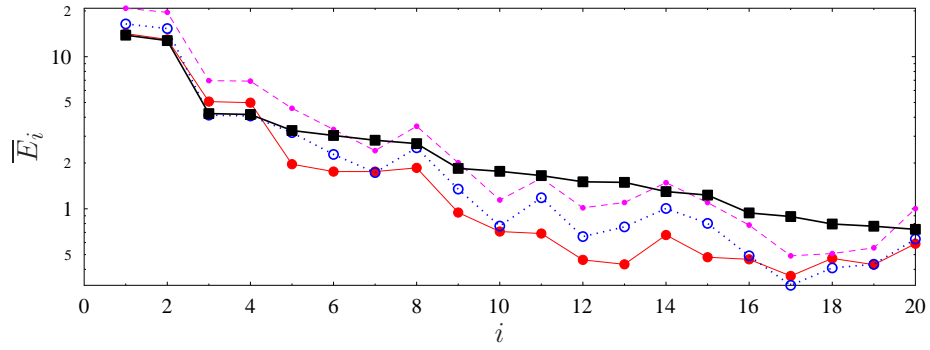


Figure 5: [Mixing layer] Optimal eddy viscosity $\nu_T^\bullet(E)$ obtained with optimization over long windows ($\Delta T = 200$; red solid line) and over short windows ($\Delta T = 10$; dashed purple line); theoretical eddy viscosity $\nu_T^\circ(E)$ is marked thick blue dotted line.



(a)



(b)

Figure 6: [Mixing layer] (a) Turbulent kinetic energy $E(t)$ as a function of time t and (b) time-averaged modal energy \bar{E}_i as a function of mode index i for DNS projected on $N = 20$ POD modes (thick black solid line), ROM with the theoretical eddy viscosity $\nu_T^\circ(E)$ (thick blue dotted line) and the optimal eddy viscosity $\nu_T^\bullet(E)$ obtained with optimization over long windows ($\Delta T = 200$; red solid line) and over short windows ($\Delta T = 10$; dashed purple line).

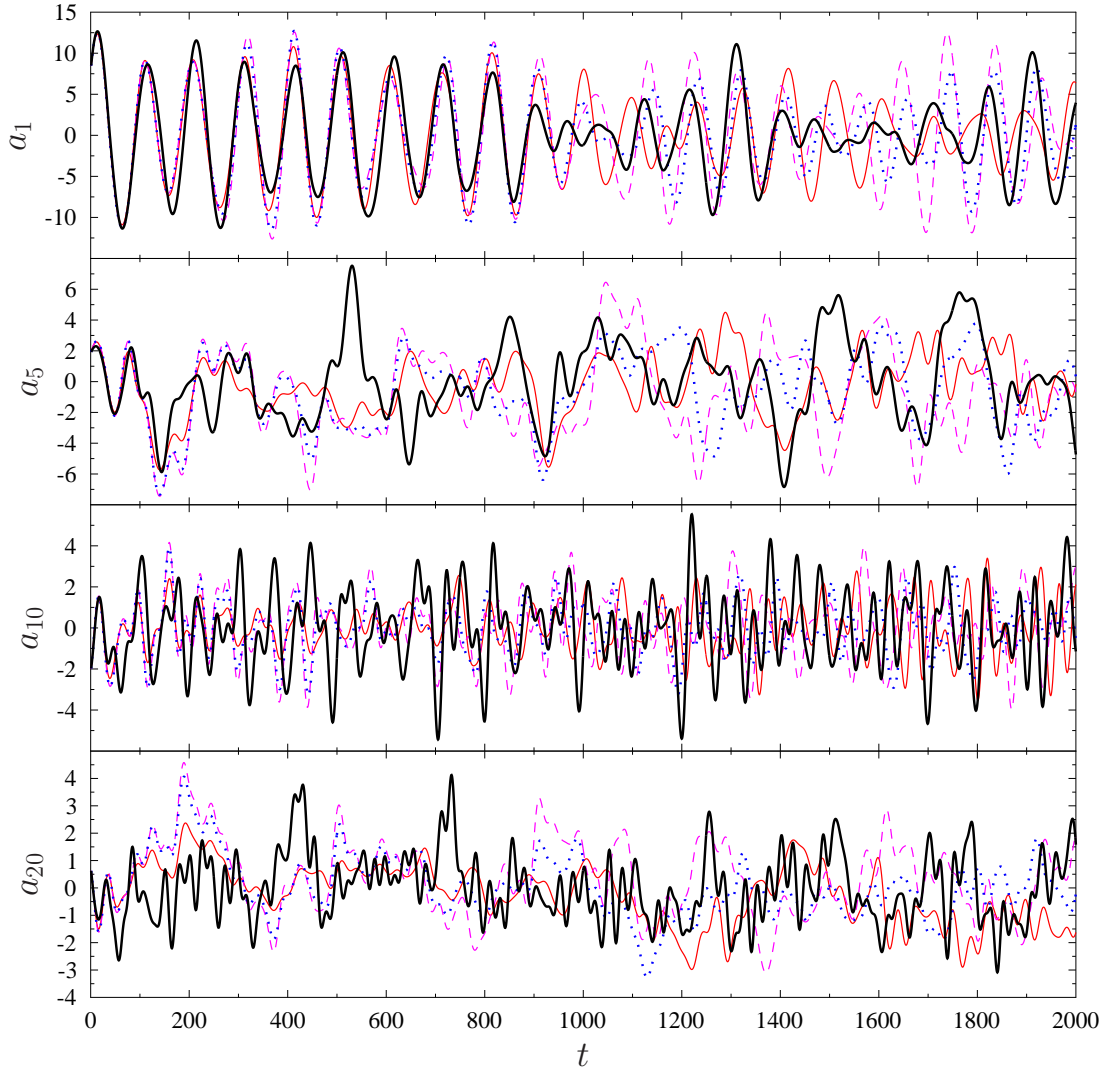


Figure 7: [Mixing layer] Galerkin expansion coefficients $a_k(t)$, $k = 1, 5, 10, 20$, as a function of time t for DNS projected on $N = 20$ POD modes (thick black solid line), ROM with the theoretical eddy viscosity $\nu_T^\circ(E)$ (thick blue dotted line) and the optimal eddy viscosity $\nu_T^\bullet(E)$ obtained with optimization over long windows ($\Delta T = 200$; red solid line) and over short windows ($\Delta T = 10$; dashed purple line).

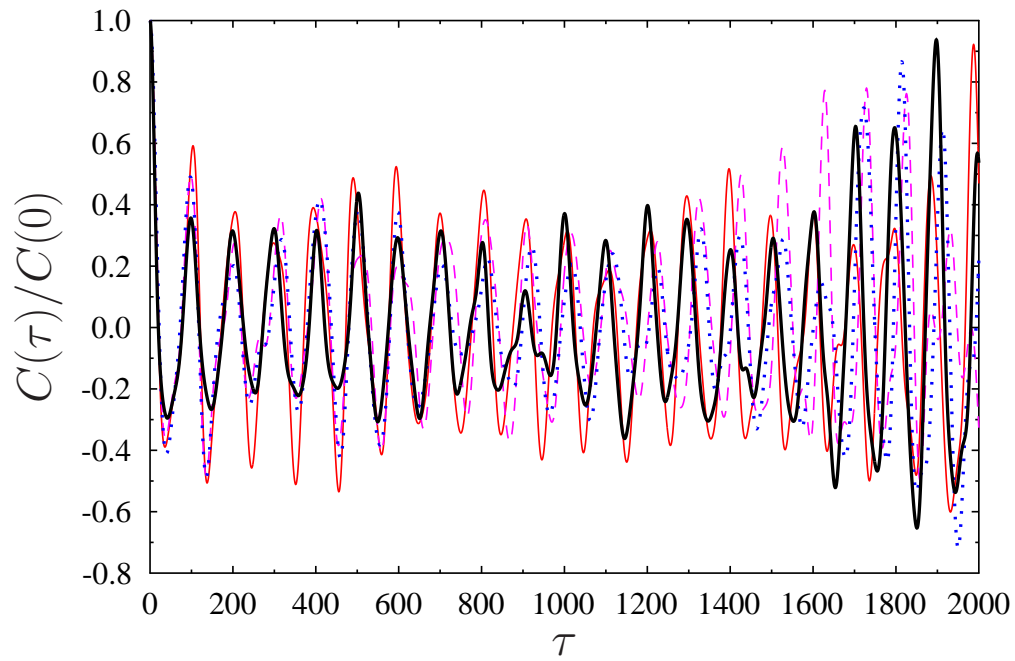


Figure 8: [Mixing layer] Normalized unbiased two-time correlation function $C(\tau)/C(0)$ for DNS projected on $N = 20$ POD modes (thick black solid line), ROM with the theoretical eddy viscosity $\nu_T^o(E)$ (thick blue dotted line) and the optimal eddy viscosity $\nu_T^*(E)$ obtained with optimization over long windows ($\Delta T = 200$; red solid line) and over short windows ($\Delta T = 10$; dashed purple line).

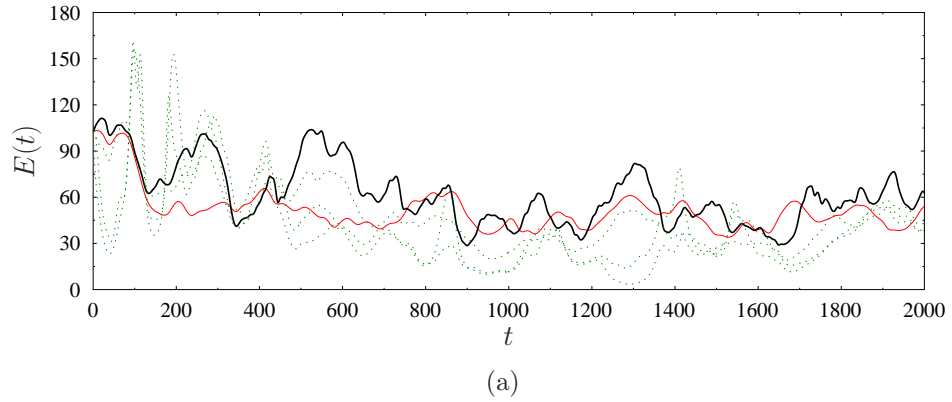


Figure 9: [Mixing layer] Comparison of turbulent kinetic energy $E(t)$ as a function of time t for DNS (thick black solid line), optimal reconstruction on long windows ($\Delta T = 200$; thin red solid line) and the results from Cordier *et al.* (2013) corresponding to three different objective functionals (dotted green lines).

Table 2: [Ahmed body] Mean resolved turbulent kinetic energy \overline{E} and its standard deviation $std(E)$ in the different cases considered in § 4.2.

	Original LES ($N = 100$)	System (11) with ν_T°	System (11) with ν_T^\bullet short windows ($\Delta T = 20$)	System (11) with ν_T^\bullet long windows ($\Delta T = 200$)
\overline{E}	0.2739	0.4514	0.3315	0.2759
$std(E)$	0.0820	0.0562	0.0504	0.0570

4.2 Ahmed body wake model

The 3D flow over the blunt Ahmed body has the Reynolds number $Re = 300,000$ based on the height $L = H$ of the body and the oncoming velocity $U = U_\infty$. The observation domain is a small wake-centered subset of the computational domain:

$$\Omega := \{(x, y, z) \in \Omega : 0 \leq x \leq 5H, -0.67H \leq y \leq 1.12H, |z| \leq 1.21H\}. \quad (34)$$

This domain is large enough to resolve the recirculation region and the absolutely unstable wake dynamics, but at the same time small enough to keep the model dimension affordable. The post-transient flow is computed over 250 convective time units, which is half of the time window analyzed by Östh *et al.* (2014), and sampled with the uniform time step $\Delta t = 1$. The reason for taking a shorter time window is that optimization problem (24) becomes hard to solve for very large T . Details of the large eddy simulation are described in Östh *et al.* (2014) and a typical flow pattern is illustrated in figure 10. The numerical data is used to construct Galerkin system (11) with dimension $N = 100$ using the procedure discussed in § 2. In contrast to the example studied in § 4.1, in the present problem with the chosen dimension $N = 100$ the Galerkin model captures only about 35% of the turbulent kinetic energy of the entire flow. We emphasize that the “target” turbulent kinetic energy $\tilde{E}(t)$ is computed based on the projection of the actual flow evolution on the first $N = 100$ modes, rather than based on the entire flow field. As in the case of the mixing layer, we will show results obtained with optimization performed over two time intervals, namely, $\Delta T = 20$ and $\Delta T = 200$, which will be referred to as the short and long window, respectively.

Decrease of cost functional (19) with iterations is shown in figure 11 in which a significant reduction can be observed in both cases. The resulting optimal eddy viscosities ν_T^\bullet are presented in figure 12, together with the theoretical model (12). We see that the obtained profile of the optimal eddy viscosity has a similar general form for both values of ΔT , except that it is smoother for the case of the longer window. This suggests that allowing for a longer assimilation interval before the constraint system (20) is restarted

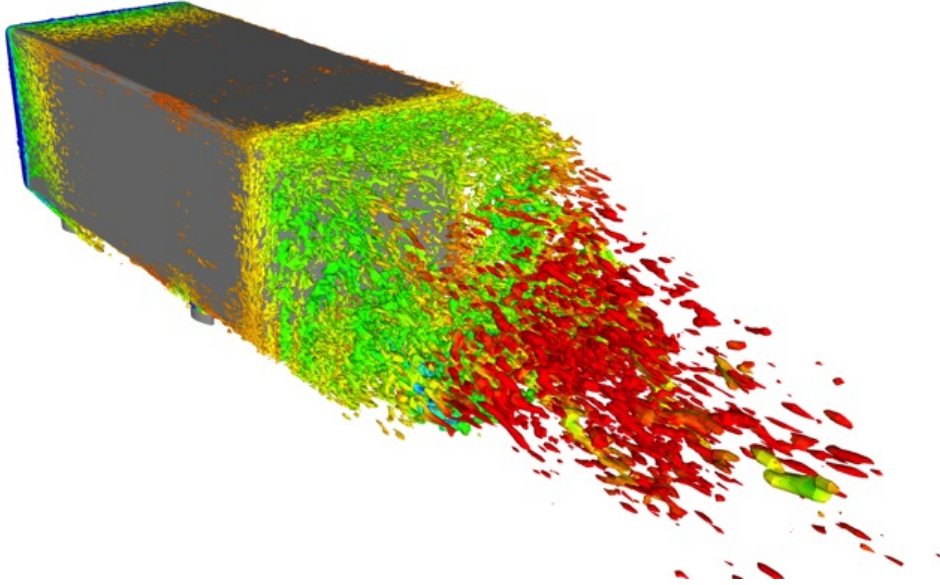


Figure 10: Illustration of a typical flow pattern in the turbulent wake behind an Ahmed body (Östh *et al.*, 2014). The flow is visualized using the quantity $Q(\mathbf{x}, t) := \boldsymbol{\omega} \cdot \boldsymbol{\omega} - \mathbf{S} : \mathbf{S}$ where $\boldsymbol{\omega} := \nabla \times \mathbf{u}$ is the vorticity and $\mathbf{S} := (1/2) [\nabla \mathbf{u} + (\nabla \mathbf{u})^T]$ is the symmetric part of the velocity gradient tensor.

with a new initial condition may have a regularizing effect. We also add that, in contrast to the findings of § 4.1, in the present case the optimal eddy viscosity ν_T^\bullet is uniformly increased with respect to the reference relation ν_T° . Figure 13a shows the improvement in the tracking of the instantaneous turbulent kinetic energy $\tilde{E}(t)$ achieved by Galerkin system (11) with the optimal eddy viscosity ν_T^\bullet with respect to the use of the theoretical relation ν_T° . The corresponding average modal energies \overline{E}_i , $i = 1, \dots, 100$, are presented in figure 13b. The observations made in figure 13 are corroborated by the mean values \overline{E} of the turbulent kinetic energy and their standard deviations collected for the different cases in Table 2. Finally, the time-histories of selected Galerkin coefficients $a_i(t)$, $i = 1, 5, 25, 100$, are shown in figure 14 and the corresponding correlation functions (32)–(33) are shown in figure 15. As is evident from the last plot, for small correlation times $\tau < 1.5$, the use of the optimal eddy viscosity ν_T^\bullet produces correlations much closer to the correlation function characterizing the original LES data.

5 Conclusions and future directions

We have proposed a novel optimal nonlinear eddy viscosity relation for a large class of reduced-order models which improves on the results from a number of earlier studies. In the pioneering investigation concerning POD-based reduced-order models by Aubry *et al.* (1988), a single constant eddy viscosity parameter was assumed. Rempfer & Fasel

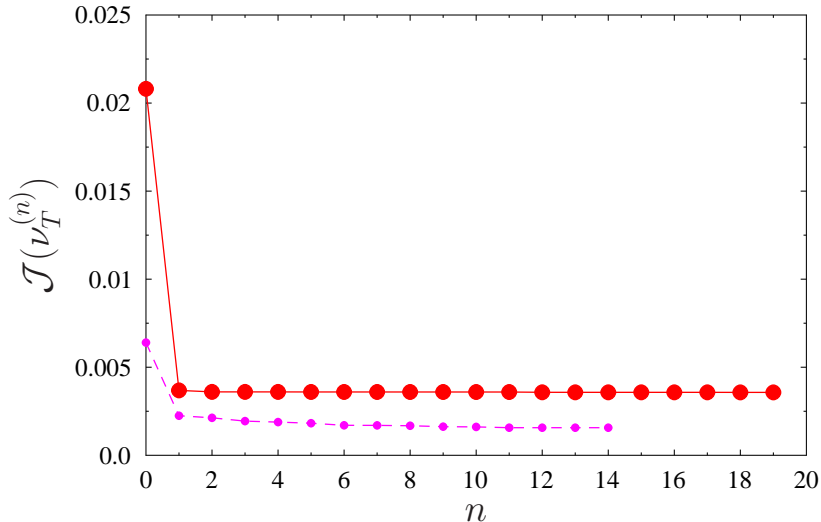


Figure 11: [Ahmed body] Decrease of the cost functional (19) with iterations n for optimization over short windows ($\Delta T = 20$; small purple symbols) and over long windows ($\Delta T = 200$; big red symbols).

(1994b) proposed a mode-dependent refinement of the constant eddy viscosity ansatz which significantly improves the accuracy of reduced-order models. Later, Noack *et al.* (2011) derived a nonlinear eddy viscosity as a function of the square root of the resolved fluctuation energy in which constant ratios between the modal energies were assumed. This nonlinearity guarantees the boundedness of the Galerkin solution (Cordier *et al.*, 2013). As shown by Östh *et al.* (2014), combinations of modal and nonlinear eddy viscosities may improve the accuracy and robustness of POD-based reduced-order models. The key new aspect of the approach proposed here is that the eddy viscosity relations are defined to be optimal in a mathematically precise sense.

The current study addresses the limitations of earlier approaches by considering the eddy viscosity as an arbitrary function of the resolved turbulent kinetic energy which is optimized by matching the fluctuation level of the reduced-order model to the corresponding quantity of the reference data. This optimization is performed with a generalization of the 4D-VAR data assimilation method adopted for the reconstruction of constitutive equations by Bukshtynov *et al.* (2011); Bukshtynov & Protas (2013).

POD models with the optimal eddy viscosity are constructed for three shear flows with progressively richer dynamics. First, the two-dimensional POD model for the transient behavior in the 2D cylinder wake is recalled from an earlier study (Protas *et al.*, 2014). Here, a negative eddy viscosity is derived at low fluctuation levels to compensate for the significantly underpredicted growth rate of the POD model. On the other hand,

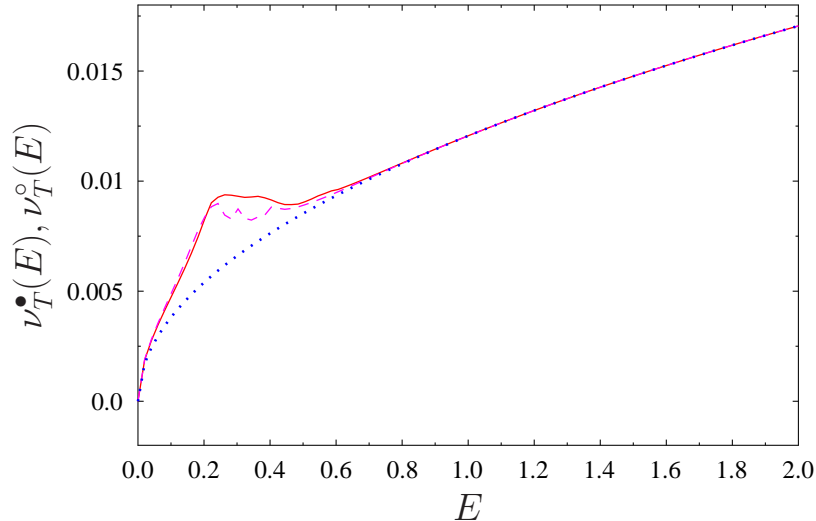
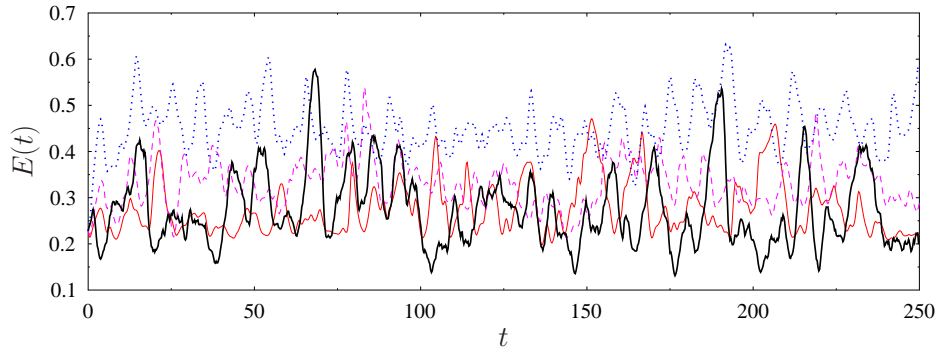


Figure 12: [Ahmed body] Optimal eddy viscosity $\nu_T^*(E)$ obtained with optimization over long windows ($\Delta T = 200$; red solid line) and over short windows ($\Delta T = 20$; dashed purple line); theoretical eddy viscosity $\nu_T^o(E)$ is marked thick blue dotted line.

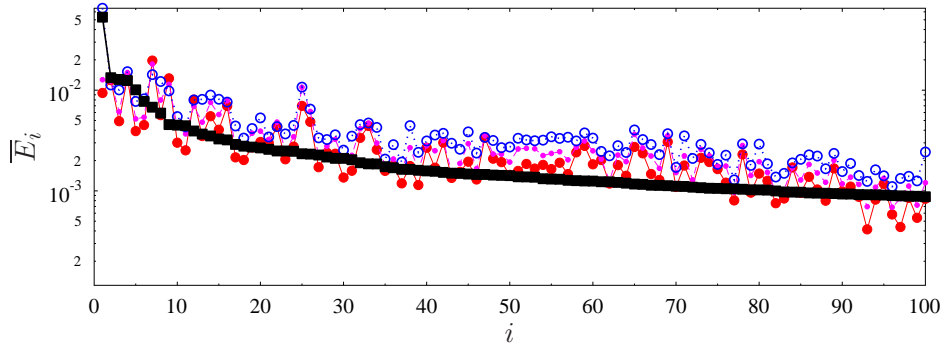
on the limit cycle and beyond, a positive eddy viscosity models the energy transfer to the higher-order modes. In this example, the eddy viscosity not only assures correct amplitudes on the limit cycle, but also yields more accurate transient times.

Second, a 20-dimensional POD model of the 2D mixing layer at $Re = 500$ with velocity ratio 3 is investigated. The starting point was a reduced-order model with a single nonlinear eddy viscosity calibrated against a DNS of the Navier-Stokes system by Cordier *et al.* (2013). Good agreement between the POD model and the DNS was observed with respect to the modal fluctuation levels and the frequency content. Surprisingly, the optimal eddy viscosity significantly deviates from the square-root ansatz (12) and attains negative values for a range of low fluctuation levels, thus accelerating the slow transients of the reduced-order model (Noack *et al.*, 2005). However, the optimal eddy viscosity ν_T^* is larger than the square-root ansatz ν_T^o at larger fluctuation levels thus limiting more energetic events.

Third, a 100-dimensional POD model of the 3D Ahmed body wake at Reynolds number 300,000 is constructed. The starting point is a large eddy simulation and the best one from the Galerkin POD models developed and analyzed by Östh *et al.* (2014, model “GS-D”) is used as a benchmark. The sub-scale turbulence representation in this model includes the modal eddy viscosities proportional to the square-root of the resolved turbulent kinetic energy (cf. §2.4). The optimal eddy viscosity respects the ratio between the modal viscosities while allowing for an arbitrary scaling with the



(a)



(b)

Figure 13: [Ahmed body] (a) Turbulent kinetic energy $E(t)$ as a function of time t and (b) time-averaged modal energy \bar{E}_i as a function of mode index i for LES projected on $N = 100$ POD modes (thick black solid line), ROM with the theoretical eddy viscosity $\nu_T^\circ(E)$ (thick blue dotted line) and the optimal eddy viscosity $\nu_T^\bullet(E)$ obtained with optimization over long windows ($\Delta T = 200$; red solid line) and over short windows ($\Delta T = 20$; dashed purple line).

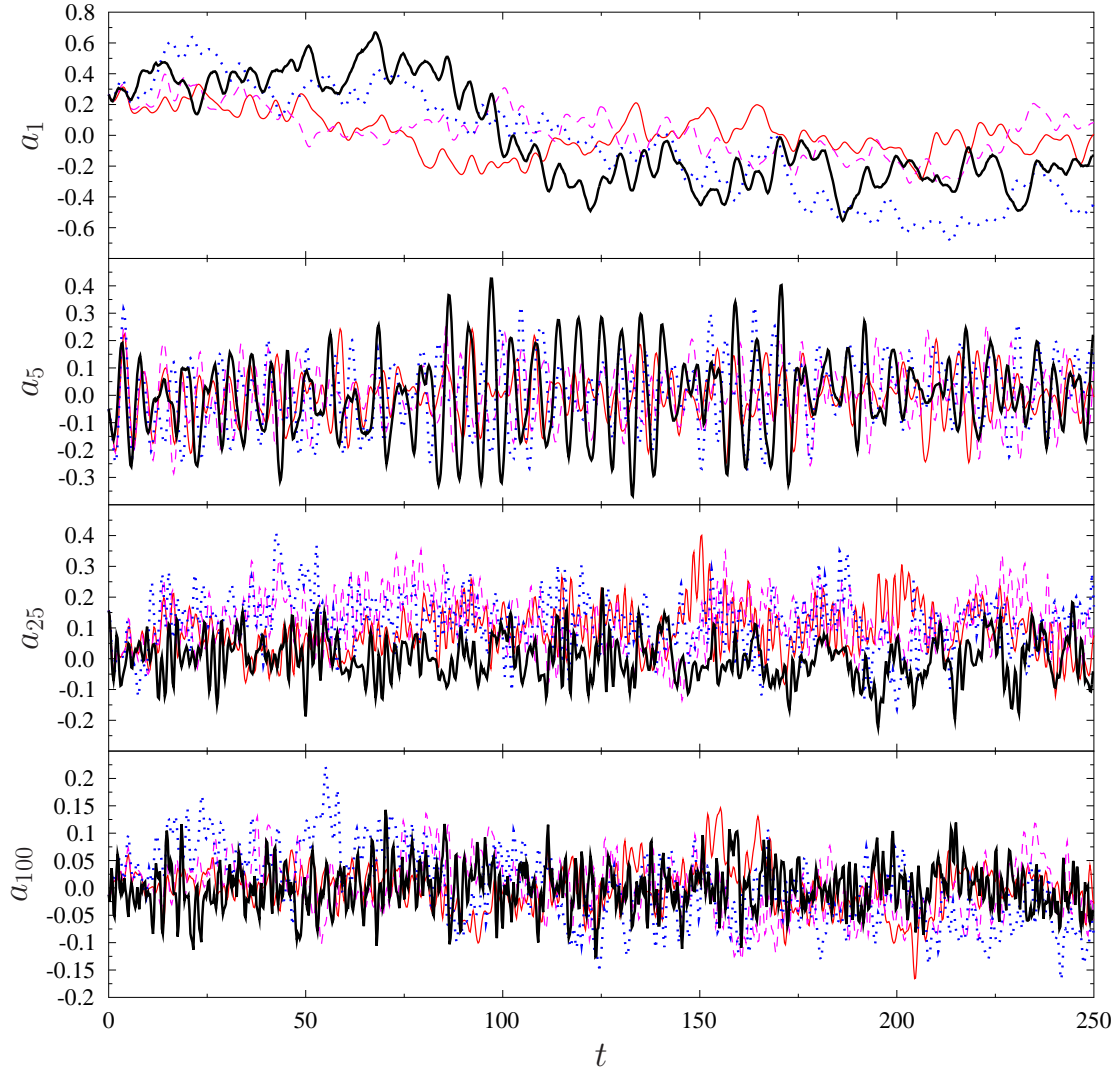


Figure 14: [Ahmed body] Galerkin expansion coefficients $a_k(t)$, $k = 1, 5, 25, 100$, as a function of time t for LES projected on $N = 100$ POD modes (thick black solid line), ROM with the theoretical eddy viscosity $\nu_T^\circ(E)$ (thick blue dotted line) and the optimal eddy viscosity $\nu_T^\bullet(E)$ obtained with optimization over long windows ($\Delta T = 200$; red solid line) and over short windows ($\Delta T = 20$; dashed purple line).

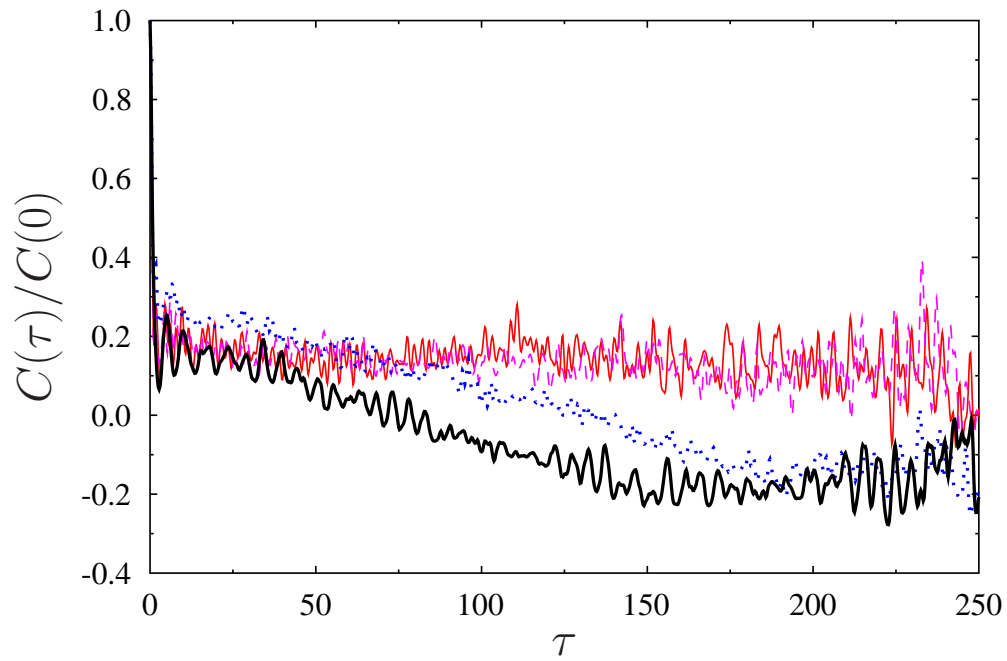


Figure 15: [Ahmed body] Normalized unbiased two-time correlation function $C(\tau)/C(0)$ for LES projected on $N = 100$ POD modes (thick black solid line), ROM with the theoretical eddy viscosity $\nu_T^o(E)$ (thick blue dotted line) and the optimal eddy viscosity $\nu_T^*(E)$ obtained with optimization over long windows ($\Delta T = 200$; red solid line) and over short windows ($\Delta T = 20$; dashed purple line).

resolved turbulent kinetic energy. As regards the comparison between the optimal and reference eddy viscosity ν_T^\bullet and ν_T° , we remark that the latter could in fact have been further improved by using solution matching techniques. For all values of the fluctuation energy the optimal eddy viscosity ν_T^\bullet exhibits larger values than the reference relation ν_T° , consistently with the overprediction of the energy fluctuation level in the latter case.

Concerning the choice of the parameters in the optimization formulation, we note that the cost functional tracking the error of the fluctuation energy gives quite comparable results over different time windows (cf. figure 2), provided that the windows cover at minimum several characteristic flow periods. This was the case for the Ahmed body flow in which the shedding period was 5-10 time units, whereas optimization was performed over intervals with $\Delta T = 20$ and $\Delta T = 200$. On the other hand, for the mixing layer the shorter window with $\Delta T = 10$ covered only half of the Kelvin-Helmholtz shedding period and the resulting optimal eddy viscosity was significantly different from the relations found by solving optimization problem (24) with subintervals 10 times longer. Given the complexity of the flow problems investigated in this study, one can expect POD models with an optimal eddy viscosity to perform well over a broad range of configurations.

The observed features of the optimal eddy viscosity identified as a function of the fluctuation energy deserve additional discussion. From the results we conjecture that the optimal eddy viscosity ν_T^\bullet does not strongly depend on the chosen time window $[0, T]$, provided that it is equal to or longer than the characteristic time scale of the dominant coherent structures. This was the case for both of the time windows used for the Ahmed body wake, but not for the short time window used for the mixing layer. Secondly, the eddy viscosity obtained for the mixing layer shows two minima helping stabilize two different energy levels. This bimodal behaviour is consistent with the cluster-based analysis of the same data performed by Kaiser *et al.* (2014). Here, it is shown that the mixing layer flow has two quasi-attractors: one which is dominated by the Kelvin-Helmholtz instability at a lower energy level and another one dominated by period-doubling at a higher energy level. Thirdly, the mixing layer model exhibits a negative eddy viscosity while the model of the Ahmed body flow does not. We conjecture that this difference has two reasons: the first is that the fluctuation levels of the mixing layer have relatively larger variations, hence we can estimate transient times for this 2D flow better than for the 3D wake; the second is that a negative eddy viscosity excites coherent structures with similar scales in the POD model of the mixing layer flow. On the other hand, for the Ahmed body wake, a negative eddy viscosity would imply that the strongly damped high-order modes would suddenly become excited which would in turn lead to an unphysical inverse energy cascade. Summarizing, the different features of the optimal eddy viscosity found for the 2D and 3D shear flows are consistent with our expectations based on the behaviour of POD models.

In providing a closure relation for unresolved fluctuations based on solution data, the proposed approach to identifying the optimal eddy viscosity bears some resemblance to the ‘‘optimal LES’’ methodology which originated with Langford & Moser (1999). However, it differs from the optimal LES in that our optimal eddy viscosity ν_T^\bullet is recon-

structured in a non-parametric manner. The proposed closure strategy can be employed in a straightforward manner to identify closure relations depending on one variable for a large class of reduced-order models. A highly relevant problem complementary to the problem solved in this study is optimization of the dependence of the eddy viscosity on the mode index i while keeping the dependence on the turbulent kinetic energy fixed. The approach developed here can be adapted to solve such problems by treating the discrete mode index i as a continuous variable, i.e., an effective wavenumber of the mode. This problem will be studied in the near future. Another related problem concerns determination of optimal turbulence closure strategies for simplified flow models defined in the PDE setting such as the RANS and LES approaches (in fact, these are the type of problems the reconstruction method we used was initially developed for, see Bukshtynov *et al.* (2011); Bukshtynov & Protas (2013)). As regards LES models, an interesting open problem is determination of optimal wall damping functions (Driest, 1956). Problems of such type also arise in fundamental turbulence research, for example, in the context of the Karman-Howarth equation. Other, possibly less obvious, extensions of this methodology include optimal identification of inertial manifolds and feedback control laws, and the authors are already pursuing these applications in the context of closed-loop turbulence control.

Acknowledgements

The authors thank Shervin Bagheri and Laurent Cordier for stimulating discussions and for providing the data used in figure 9 (L.C.). Funding for this research was provided by the French Agence Nationale de la Recherche (ANR) via the Chair of Excellence TUCOROM and is gratefully acknowledged. B.P. was also partially supported by a Discovery Grant from the Natural Sciences and Engineering Research Council of Canada (NSERC). A part of this work was based on J. Östh’s Ph.D. thesis which was financially supported by Trafikverket (Swedish Transport Administration).

A Derivation of Gradient Expression

In this appendix we derive expression (28) for the L_2 gradient of cost functional (19). The key observation is that, since the Gâteaux differential of $\mathcal{J}(\nu_T)$ appearing in (25) is a bounded linear functional with respect to its second argument $\nu'_T \in \mathcal{X}(\mathcal{I})$, $\mathcal{X}(\mathcal{I})$ being an appropriate Hilbert function space, by the Riesz representation theorem (Berger, 1977) we have

$$\forall \nu'_T \in \mathcal{X}(\mathcal{I}) \quad \mathcal{J}'(\nu_T; \nu'_T) = \left\langle \nabla^{\mathcal{X}} \mathcal{J}, \nu'_T \right\rangle_{\mathcal{X}(\mathcal{I})}, \quad (35)$$

where $\langle \cdot, \cdot \rangle_{\mathcal{X}(\mathcal{I})}$ denotes the inner product in the space $\mathcal{X}(\mathcal{I})$. We identify the Riesz representer $\nabla^{\mathcal{X}} \mathcal{J}$ as the *gradient* of \mathcal{J} with respect to the topology of the space $\mathcal{X}(\mathcal{I})$ (in the present problem, we have either $\mathcal{X}(\mathcal{I}) = L_2(\mathcal{I})$ or $\mathcal{X}(\mathcal{I}) = H^1(\mathcal{I})$). We begin by

computing the Gâteaux differential of (19) which yields

$$\mathcal{J}'(\nu_T; \nu'_T) = \frac{1}{T} \int_0^T [E(t) - \tilde{E}(t)] E'(t) dt = \frac{1}{T} \int_0^T [E(t) - \tilde{E}(t)] \sum_{i=1}^N a_i(t) a'_i(t) dt, \quad (36)$$

where $E' := \sum_{i=1}^N a_i a'_i$ and a'_i , $i = 1, \dots, N$, solve the linearization of system (20). Following the approach described by Protas *et al.* (2014), this linearization can be shown to have the form

$$\begin{aligned} \frac{da'_i}{dt} &= \sum_{j=0}^N \left[\sum_{k=0}^N (q_{ijk} + q_{ikj}) a_k + l'_{ij} \left(\nu + \nu_T(E(t)) + \frac{d\nu_T}{de} a_i a_j \right) \right] a'_j + \nu'_T(E(t)) \sum_{j=0}^N l'_{ij} a_j, \\ &=: \sum_{j=0}^N A_{ij} a'_j + \nu'_T(E(t)) \sum_{j=0}^N l'_{ij} a_j, \quad t \in ((m-1)\Delta T, m\Delta T] \end{aligned} \quad (37a)$$

$$a'_0(t) = 0, \quad (37b)$$

$$a'_i((m-1)\Delta T) = 0, \quad i = 1, \dots, N, \quad m = 1, \dots, M, \quad (37c)$$

where the second line in (37a) defines the linear operator \mathbf{A} . We note that differential (36) is not yet in a form consistent with Riesz representation (35), because the perturbation variable ν'_T does not enter as a linear factor in (36), but is instead hidden in a source term in equation (37a). In order to transform (36) into Riesz form (35), we introduce the *adjoint state* $\mathbf{a}^*(t) = [0, a_1^*(t), \dots, a_N^*(t)]^T \in \mathbb{R}^{N+1}$, so that integrating it against perturbation equation (37a) and applying integration by parts we obtain

$$\begin{aligned} &\sum_{i=1}^N \int_0^T \left(\frac{da'_i}{dt} - \sum_{j=0}^N A_{ij} a'_j - \nu'_T(E(t)) \sum_{j=0}^N l'_{ij} a_j \right) a_i^* dt = \\ &\sum_{i=1}^N a'_i a_i^* \Big|_{t=0}^{t=T} + \sum_{i=1}^N \int_0^T a'_i \left(-\frac{da_i^*}{dt} - \sum_{j=0}^N A_{ji} a_j^* \right) dt - \int_0^T \nu'_T(E(t)) \sum_{i=1, j=0}^N l'_{ij} a_j a_i^* dt = 0. \end{aligned} \quad (38)$$

Since $a_0^*(t) \equiv 0$, summation over index i in (38) starts at 1. Defining the *adjoint system* as in (29), and using it together with (36) and (37), we obtain from (38)

$$\mathcal{J}'(\nu_T; \nu'_T) = \int_0^T \nu'_T(E(t)) \sum_{i,j=0}^N l'_{ij} a_j a_i^* dt. \quad (39)$$

In order to transform this expression to the Riesz form induced by $\mathcal{X}(I) = L_2(\mathcal{I})$, i.e.,

$$\mathcal{J}'(\nu_T; \nu'_T) = \int_0^{E_{\max}} \nabla^{L_2} \mathcal{J} \nu'_T de, \quad (40)$$

we need to change the integration variable in (39) from time t to turbulent kinetic energy e

$$\begin{aligned} \frac{de}{dt} &= \sum_{i=1}^N a_i \frac{da_i}{dt} = \sum_{i=1}^N a_i \left(f_i(\mathbf{a}) + \nu_T(E(t)) \sum_{j=0}^N l_{ij}^\nu a_j \right) \\ \implies dt &= \frac{de}{\sum_{i=1}^N a_i \left(f_i(\mathbf{a}) + \nu_T(E(t)) \sum_{j=0}^N l_{ij}^\nu a_j \right)}, \end{aligned} \quad (41)$$

so that Gâteaux differential (39) becomes

$$\begin{aligned} \mathcal{J}'(\nu_T; \nu_T') &= \int_{\mathcal{C}} \frac{\sum_{i,j=0}^N l_{ij}^\nu a_j a_i^*}{\sum_{i=1}^N a_i \left(f_i(\mathbf{a}) + \nu_T(E(t)) \sum_{j=0}^N l_{ij}^\nu a_j \right)} \nu_T'(e) de \\ &= \int_0^{E_{\max}} \sum_{\substack{t \\ E(\mathbf{a}(t))=e}} \frac{\sum_{i,j=0}^N l_{ij}^\nu a_j a_i^*}{\sum_{i=1}^N |a_i f_i(\mathbf{a}) + \nu_T(E(t)) \sum_{j=0}^N l_{ij}^\nu a_j|} \nu_T'(e) de, \end{aligned} \quad (42)$$

where the first expression on the right-hand side in (42) is an integral over the system trajectory \mathcal{C} in the phase space \mathbb{R}^n (i.e., a *line* integral in which de can be either positive or negative), whereas the second expression is a *definite* integral consistent with Riesz form (40). Thus, identifying (42) with (40), we finally obtain gradient expression (28).

References

- ADAMS, R. A. & FOURNIER, J. F. 2005 *Sobolev Spaces*. Elsevier.
- ARTANA, G., CAMMILLERI, A., CARLIER, J. & MÉMIN, E. 2012 Strong and weak constraint variational assimilations for reduced-order fluid flow modeling. *J. Comp. Phys.* **231**, 3264–3288.
- AUBRY, N. HOLMES, P. LUMLEY, J. L. & STONE, E. 1988 The dynamics of coherent structures in the wall region of a turbulent boundary layer. *J. Fluid Mech.* **192**, 115–173.
- BALAJEWICZ, M., DOWELL, E. H. & NOACK, B. R. 2013 Low-dimensional modelling of high-Reynolds-number shear flows incorporating constraints from the Navier-Stokes equation. *J. Fluid Mech.* **729**, 285–308.
- BERGER, M. S. 1977 *Nonlinearity and Functional Analysis*. Academic Press.
- BUKSHTYNOV, V. & PROTAS, B. 2013 Optimal reconstruction of material properties in complex multiphysics phenomena. *J. Comp. Phys.* **242**, 889–914.
- BUKSHTYNOV, V., VOLKOV, O. & PROTAS, B. 2011 On optimal reconstruction of constitutive relations. *Physica D* **240**, 1228–1244.

- CACUCI, D. G. NAVON, I. M. & IONESCU-BUJOR, M. 2013 *Computational Methods for Data Evaluation and Assimilation*. Oxford, UK: Chapman & Hall.
- CORDIER, L. NOACK, B. R. DAVILLER, G. DELVILE, J. LEHNASCH, G. TISSOT, G. BALAJEWICZ, M. & NIVEN, R.K. 2013 Control-oriented model identification strategy. *Exp. Fluids* **54**, Article 1580.
- D’ADAMO, J., PAPADAKIS, N., MÉMIN, E. & ARTANA, G. 2007 Variational assimilation of POD low-order dynamical systems. *J. Turb.* **9**, 1–22.
- DEANE, A. E. KEVREKIDIS, I. G. KARNIADAKIS, G. E. & ORSZAG, S. A. 1991 Low-dimensional models for complex geometry flows: Application to grooved channels and circular cylinders. *Phys. Fluids A* **3**, 2337–2354.
- DRIEST, E.R. VAN 1956 On turbulent flow near a wall. *J. Aero. Sci.* **23**, 1007.
- FLETCHER, C. A. J. 1984 *Computational Galerkin Methods*, 1st edn. New York: Springer.
- GALLETTI, G. BRUNEAU, C. H. ZANNETTI, L. & IOLLO, A. 2004 Low-order modelling of laminar flow regimes past a confined square cylinder. *J. Fluid Mech.* **503**, 161–170.
- GUNZBURGER, M. D. 2003 *Perspectives in Flow Control and Optimization*. SIAM.
- HEMATI, M. S., ELDREDGE, J. D. & SPEYER, J. L. 2014 Improving vortex models via optimal control theory. *J. Fluids Struct.* (in print).
- HOLMES, P. LUMLEY, J. L. BERKOOZ, G. & ROWLEY, C. W. 2012 *Turbulence, Coherent Structures, Dynamical Systems and Symmetry*, 2nd edn. Cambridge: Cambridge University Press.
- KAISER, E. NOACK, B. R. CORDIER, L. SPOHN, A. SEGOND, M. ABEL, M. W. DAVILLER, G. ÖSTH, J. KRAJNOVIĆ, S. & NIVEN, R. K. 2014 Cluster-based reduced-order modelling of a mixing layer. *J. Fluid Mech.* (in print).
- KASTEN, J. REININGHAUS, J. HOTZ, I. HEGE, H.-C. NOACK, B. R. DAVILLER, G. COMTE, P. & MORZYŃSKI, M. 2014 Acceleration feature points of unsteady shear flows. *Tech. Rep.* 1401.2462 [physics.fui-dyn]. arXiv.
- KUTZ, J. N. 2013 *Data-Driven Modeling & Scientific Computation: Methods for Complex Systems & Big Data*. Oxford University Press.
- LAMB, SIR H. 1945 *Hydrodynamics*, 6th edn. New York: Dover Publications.
- LANGFORD, J. A. & MOSER, R. D. 1999 Optimal LES formulations for isotropic turbulence. *Journal of Fluid Mechanics* **398**, 321–346.

- LIBERZON, A., LÜTHI, B., GUALA, M., KINZELBACH, W. & TSINOBER, A. 2007 On anisotropy of turbulent flows in regions of "negative eddy viscosity". In *Progress in Turbulence II, Proceedings of the iTi Conference in Turbulence 2005* (ed. M. Oberlack, G. Khujadze, S. Günther and T. Weller, M. Frewer, J. Peinke & S. Barth), *Springer Proceedings in Physics*, vol. 109. Springer.
- LUENBERGER, D. 1969 *Optimization by Vector Space Methods*. John Wiley and Sons.
- LUMLEY, J.L. 1970 *Stochastic Tools in Turbulence*. New York: Academic Press.
- MA, X. & KARNIADAKIS, G. E. 2002 A low-dimensional model for simulating three-dimensional cylinder flow. *J. Fluid Mech.* **458**, 181–190.
- NOACK, B. R. AFANASIEV, K. MORZYŃSKI, M. TADMOR, G. & THIELE, F. 2003 A hierarchy of low-dimensional models for the transient and post-transient cylinder wake. *J. Fluid Mech.* **497**, 335–363.
- NOACK, B. R. MORZYŃSKI, M. & TADMOR, G. 2011 *Reduced-Order Modelling for Flow Control. CISM Courses and Lectures* 528. Vienna: Springer-Verlag.
- NOACK, B. R. PAPAS, P. & MONKEWITZ, P. A. 2005 The need for a pressure-term representation in empirical Galerkin models of incompressible shear flows. *J. Fluid Mech.* **523**, 339–365.
- NOCEDAL, J. & WRIGHT, S. 2002 *Numerical Optimization*. Springer.
- ORFANIDIS, S. J. 1996 *Optimum Signal Processing. An Introduction.*, 2nd edn. Prentice-Hall.
- ÖSTH, J., NOACK, B. R., KRAJNOVIĆ, S., BARROS, D. & BORÉE, J. 2014 On the need for a nonlinear subscale turbulence term in pod models as exemplified for a high reynolds number flow over an ahmed body. *Journal of Fluid Mechanics* **747**, 518–544.
- PODVIN, B. 2009 A proper-orthogonal-decomposition based model for the wall layer of a turbulent channel flow. *Phys. Fluids* **21**, 015111–1..18.
- PRESS, W. H., FLANNER, B. P., TEUKOLSKY, S. A. & VETTERLING, W. T. 1986 *Numerical Recipes: the Art of Scientific Computations*. Cambridge University Press.
- PROTAS, B., BEWLEY, T. & HAGEN, G. 2004 A comprehensive framework for the regularization of adjoint analysis in multiscale pde systems. *J. Comp. Phys.* **195**, 49–89.
- PROTAS, B., NOACK, B. R. & MORZYNSKI, M. 2014 An optimal model identification for oscillatory dynamics with a stable limit cycle. *J. Nonlin. Sci.* **24**, 245–275.
- REMPFER, D. & FASEL, F.H. 1994a Evolution of three-dimensional coherent structures in a flat-plate boundary-layer. *J. Fluid Mech.* **260**, 351–375.

- REMPFER, D. & FASEL, F. H. 1994*b* Dynamics of three-dimensional coherent structures in a flat-plate boundary-layer. *J. Fluid Mech.* **275**, 257–283.
- SAPSIS, T. P. & MAJDA, A.J. 2013 Statistically accurate low-order models for uncertainty quantification in turbulent dynamical systems. *Proc. Natl. Acad. Sci USA* **110**, 13705–13710.
- SIROVICH, L. 1987 Turbulence and the dynamics of coherent structures, Part I: Coherent structures. *Quart. Appl. Math.* **XLV**, 561–571.
- WANG, Z. AKHTAR, I. BORGGAARD, J. & ILIESCU, T. 2011 Two-level discretizations of nonlinear closure models for proper orthogonal decomposition. *J. Comp. Phys.* **230**, 126–146.
- WANG, Z., AKHTAR, I., BORGGAARD, J. & ILIESCU, T. 2012 Proper orthogonal decomposition closure models for turbulent flows: A numerical comparison. *Comput. Methods Appl. Mech. Engrg.* **237-240**, 10–26.